

Performance Evaluation for Robust Control of Spatial Disturbances in Channel Flow

Enda O'Dea, Owen R. Tutty, Eric Rogers

Abstract—The systems dealt with in flow control problems are, in control terms, very complex, nonlinear and infinite dimensional, even if the fluid flow is comparatively simple. Plane Poiseuille flow, i.e. flow between two infinite parallel plates is one of the simplest and best understood cases of fluid dynamics. Controlling this flow is, however, still a very challenging problem, even if it is assumed that deviations from the steady-state are small enough for the governing equations to be linearized. Recent work has shown that robust control of 2D channel flow is possible without a spatial periodicity assumption.

This paper will first execute an H_∞ based robust control law design for the 2D case and then proceed to the relatively open problem of assessing the resulting performance using a Navier Stokes CFD solver as a model of the 'real' process. The results in this second part will be on the representation (to ensure realistic results) and modelling of the disturbances used and the control of 3D disturbances.

I. INTRODUCTION

Recently flow control has attracted considerable attention in the fluids research community. One of the motivations comes from the possibility of reducing drag on a body by preventing or delaying transition from laminar to turbulent flow. The systems dealt with in these problems are, in control terms, very complex, nonlinear and infinite dimensional, even if the fluid flow is comparatively simple. Plane Poiseuille flow, i.e. flow between two infinite parallel plates is one of the simplest and best understood cases of fluid dynamics. Controlling this flow is, however, still a challenging problem, even if it is assumed that deviations from the steady-state are small enough for the governing equations to be linearized.

It has become a benchmark problem for developing control algorithms for fluid flows and was considered in [1], [2], [3], [4] among others. All these references make an assumption that the flow is spatially periodical in the streamwise direction and subsequently, they use Fourier-Galerkin decomposition to obtain independent dynamics for each respective Fourier mode.

An interesting result is in [5] where tangential blowing and suction was used instead of the normal one. Distributed actuation and sensing was considered and a nonlinear decentralized controller was developed. Conversely, this method is applicable only for a limited range of viscosities.

Enda O'Dea is with the Meteorological Office, Exeter, UK, enda.odea@metoffice.gov.uk

Owen Tutty is with the School of Engineering Sciences, University of Southampton, Southampton, SO17 1BJ, UK, ort@soton.ac.uk

Eric Rogers is with the School of Electronics and Computer Science, University of Southampton, Southampton, SO17 1BJ, UK, etar@ecs.soton.ac.uk

In [6], boundary control for 'discrete' transpiration was proposed, where blowing and suction takes place only along short, periodically spaced sections of the wall. It is a model of blowing/suction panels which are being developed and considered for use in the aerospace industry. Then, assuming point measurements, a reduced order multi-wavenumber flow model was obtained. The modelling uncertainty was estimated and taken into account in the H_∞ control design.

In this paper we shall *not* impose the periodicity assumption and we shall consider control of a *spatially growing* flow. This practically important issue has not been addressed directly before, to the best of our knowledge. We shall consider again the boundary control in the form of blowing/suction panels and discrete-points measurements. Specifically, we shall use four regularly spaced blowing/suction panels and five sensors—which is sufficient to reduce the wall-shear stress significantly near the actuation/sensing area and slow down its growth further downstream. In this setting we cannot apply Fourier decomposition and use finite differences instead. By a technique based on the Redheffer star product we obtain (pointwise) frequency-response data of the flow. A low-order model is then fitted on these data. A modelling uncertainty is estimated using a LMI-based procedure. This procedure is derived from the frequency-domain model validation ideas of [7]. Finally, a robustly stable H_∞ controller is designed for this model set.

The control design is tested in simulations with a nonlinear Navier-Stokes solver in the loop and the main results are reported in this paper. This paper will also give recent results on the representation (to ensure realistic results) and modelling of the disturbances used and the control of 3D disturbances.

II. BACKGROUND

We consider a planar flow in an infinite channel of fixed height. The flow is non-dimensionalised using the channel half-height and the center-line velocity. We consider a coordinate system as in Figure 1.

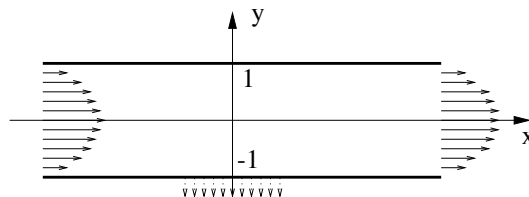


Fig. 1. Coordinate system.

Let $p(x, y, t)$ be the pressure and, $u(x, y, t)$ and $v(x, y, t)$ be the velocities in the direction of x and y axes, respectively. The steady base flow is given by $p(x, y, t) = -2x/Re$, $u(x, y, t) = 1 - y^2 =: U(y)$ and $v(x, y, t) = 0$ where Re is the Reynolds number. Assume that the quantities $\hat{p}(x, y, t) \equiv p(x, y, t) + 2x/Re$, $\hat{u}(x, y, t) \equiv u(x, y, t) - U(y)$, and $\hat{v}(x, y, t) \equiv v(x, y, t)$ are small so flow is governed by the linearized Navier-Stokes equations

$$\frac{\partial \hat{u}}{\partial t} + U \frac{\partial \hat{u}}{\partial x} + \frac{dU}{dy} \hat{v} = -\frac{\partial \hat{p}}{\partial x} + \frac{1}{Re} \nabla^2 \hat{u} \quad (1)$$

$$\frac{\partial \hat{v}}{\partial t} + U \frac{\partial \hat{v}}{\partial x} = -\frac{\partial \hat{p}}{\partial y} + \frac{1}{Re} \nabla^2 \hat{v} \quad (2)$$

$$\frac{\partial \hat{u}}{\partial x} + \frac{\partial \hat{v}}{\partial y} = 0 \quad (3)$$

where $\nabla^2 = \partial^2/\partial x^2 + \partial^2/\partial y^2$. The boundary conditions are $\hat{u}(x, 1, t) = \hat{v}(x, 1, t) = 0$, $\hat{u}(x, -1, t) = 0$ and $\hat{v}(x, -1, t) = -(dl(x)/dx)$. The last condition describes the wall-normal blowing/suction. The function $l(x)$ represents the geometric configuration of the blowing and suction elements. The function $q(t)$ modifies the blowing/suction according to the control law—it is the normalized suction velocity through the wall. In the case of several independent actuators we may consider q to be an m -dimensional column vector and l an $(1, m)$ -dimensional matrix.

To write the Navier-Stokes equations into the form used in this study, we use the so-called modified stream function as in e.g. [1]. Then a finite-dimensional approximation of the result is obtained using (as in other work) a Chebyshev expansion in the cross-channel direction and, since we do not impose the periodicity assumption, finite-differences instead of the Fourier expansion in the streamwise direction. Suppose that the x -coordinate is discretized by regularly spaced samples $\{x_n, n = \dots, -1, 0, 1, \dots\}$ and let $\delta = x_n - x_{n-1}$. Then, approximating the partial derivatives present by symmetric differences and a Galerkin procedure (see [8]) we produce (the details are in [9]) for the n -th grid point a set of $2(M+1)$ ordinary first order equations which can be written as

$$\begin{aligned} \dot{x}_n &= Ax_n + B_{1n}q + B_{2n}\dot{q} + B_{-2}x_{n-2} \\ &+ B_{-1}x_{n-1} + \hat{B}_{-1}\dot{x}_{n-1} \\ &+ B_{+1}x_{n+1} + \hat{B}_{+1}\dot{x}_{n+1} + B_{+2}x_{n+2} \end{aligned} \quad (4)$$

where $\mathbf{x}_n = [\xi_{n0} \ \dots \ \xi_{nM}]^T$. Notice that the matrices above are the same for all grid points, except for B_{1n} and B_{2n} which express the effect of the boundary input and depend on $l(x_{n-2}), \dots, l(x_{n+2})$.

The output approximating shear at the n -th gridpoint becomes

$$z_n = \sum_{n=-N}^N Cx_n + D_nq \quad (5)$$

To condense the notation, we combine the equations for a set of 5 grid points as

$$\dot{x}_{sn} = A_s x_{sn} + B_{1n} v_{ib}^n + B_{2n} v_{if}^n \quad (6)$$

where

$$x_{sn} = \begin{bmatrix} x_n \\ \vdots \\ x_{n+4} \end{bmatrix}, \quad v_{ib}^n = \begin{bmatrix} x_{n-2} \\ x_{n-1} \\ \dot{x}_{n-1} \\ q \\ \dot{q} \end{bmatrix}$$

and

$$v_{if}^n = \begin{bmatrix} x_{n+6} \\ x_{n+5} \\ \dot{x}_{n+5} \end{bmatrix}$$

Here the sub-script *ib* and *if* stand for input-back and input-forward, respectively. The outputs fed-back and fed-forward from this system are denoted by

$$v_{ob}^n = \begin{bmatrix} x_{n+1} \\ x_n \\ \dot{x}_n \\ q \\ \dot{q} \end{bmatrix}, \quad v_{of}^n = \begin{bmatrix} x_{n+3} \\ x_{n+4} \\ \dot{x}_{n+4} \\ q \\ \dot{q} \end{bmatrix} \quad (7)$$

These equations approximate the behavior of a channel segment over 5 grid points, i.e. of length 4δ . We can conveniently form the transfer matrix $G^n(s)$ mapping Laplace transform images of v_{ib}^n, v_{if}^n to the Laplace images of v_{ob}^n, v_{of}^n . To get a model of two adjacent segments of total length 9δ we need a feedback interconnection of $G^n(s)$ and $G^{n+5}(s)$ in the form of a Redheffer Star Product and denoted as $G^n * G^{n+5}$. Then, a long stretch of the channel flow is obtained as a chain of star products,

$$G^{n-5N_1}(s) * \dots * G^n(s) * G^{n+5}(s) * \dots * G^{n+5N_2}(s) \quad (8)$$

Theoretically, a state-space representation of a channel could be build up this way as well, but that would require huge computational costs and storing enormous amount of data which would be of little use afterwards. Instead, we shall store only frequency domain data, so the above cascade of star products is computed pointwise, for a finite set of $\{j\omega_i, i = 1, \dots, K\}$. Star-product over complex matrices is a simple operation. Low-order transfer functions from the boundary input to the shear output will be fitted on this frequency-domain data.

The boundary conditions at the up- and down-stream ends of the channel can be described as transfer matrices from $v_{ob}^{n-5N_1}$ to $v_{ib}^{n-5N_1}$ and $v_{of}^{n+5N_2}$ to $v_{if}^{n+5N_1}$, respectively. In our case, we shall leave them zero and consider a long enough channel so the conditions at its ends have an negligible effect on the relevant mid-section. On the other hand, if we connected $v_{ib}^{n-5N_1}$ with $v_{of}^{n+5N_2}$ and $v_{if}^{n+5N_1}$ with $v_{ob}^{n-5N_1}$ we would obtain the periodic case, studied in, for example, [1], [2], [3].

We assume that the dynamics of the actuator is described by

$$\dot{x}_p = A_p x_p + B_p u, \quad q = C_p x_p \quad (9)$$

where u is the control input. The derivative of q is then obtained as

$$\dot{q} = C_p A_p x_p + C_p B_p u \quad (10)$$

In the following, we shall consider an actuator model of $A_p = -1$, $B_p = 100$ and $C_p = 1$. We take $Re = 10^4$.

As for the controlled boundary condition, we consider $dl(x)/dx$ a rectangular pulse of width 0.5π and height 1. The function $l(x)$ is zero at the upstream end. This function is a model of blowing/suction panels which are under development and considered for use in the aerospace industry.

Strictly speaking, this function is not smooth enough and hence the defining PDE has singularities at points where $dl(x)/dx$ is not continuous. Because of the non-zero grid size, the numerical procedure overcomes these singularities. This affects shear output data from channel segments containing this singularities; elsewhere, the data converge well as $\delta \rightarrow 0$. Hence, we must avoid these points when placing shear sensors.

Up to now we have been discussing single-input-single-output system; however, with no loss of generality, we can obtain frequency-domain data directly from the scalar case. Consider there is a set of k sensors regularly spaced in the intervals of δ_s and a set of m panels with a distance δ_p between their centers, we can get the transfer matrix $G_{uz}(s) = [G_{uz}(s, x + (i-1)\delta_s + (1-j)\delta_p)]_{i=1, \dots, k; j=1, \dots, m}$ where the scalar function $G_{uz}(s, x)$ is as in the previous section; x is now fixed. In what follows we shall consider $\delta_s = \delta_k = \pi$. This separation between panels/sensors is chosen so that the controller can most efficiently attack the disturbance of 2π wavelength. The constant x was chosen as $x = 6.2\pi$ which means that sensors are placed at the distance of 0.2π downstream from the panels.

Each of the above transfer matrices is chosen as an N_{ij} -order proper rational function. This separation between panels/sensors is chosen so that the controller can most efficiently attack the disturbance of 2π wavelength. The constant x was chosen as $x = 6.2\pi$ which means that sensors are placed at the distance of 0.2π downstream from the panels.

For uncertainty representation we use the well known left-coprime factor uncertainty. Let the low-order representation of the flow, obtained from the fitting procedure be $\hat{G}_{uz}(s)$ and its left-coprime factorization $\hat{G}_{uz}(s) = M(s)^{-1}N(s)$. One possible choice is the *normalized left-coprime factorization*. Then, we shall consider the model set

$$\{(M + W_1\Delta_1W_2)^{-1}(N + W_1\Delta_2W_3)\} \quad (11)$$

such that Δ_1, Δ_2 stable, $\|[\Delta_1, \Delta_2]\|_\infty < 1$. Here W_1, W_2, W_3 are stable and minimum phase weighting matrices. First, we shall consider the following problem: given fixed weights and set of frequency points $\{\omega_i\}_{i=1}^k$, are the data $G_{uz}(j\omega_i)$, $i = 1, \dots, K$ consistent with the model? The details of how the consistency of this model is checked can be found in [9]. In the following, for the sake of simplicity, we shall restrict ourselves to diagonal weights with W_1 a constant, W_2 band-pass and W_4 band-stop.

For control system design we need a disturbance model. Although its accuracy does not affect the closed-loop stability (and hence its error is not included to the overall

modelling uncertainty) it is important for the performance. First we consider the problem: If we measure the shear disturbance at a point x , can we estimate the value of shear at $x + \Delta_x$ at the same time? The answer is yes, provided it is far downstream from its source and Δ_x is close to the basic wavelengths for the fast growing components (i.e. approx 2π) (or their integer multiples). Hence we use

$$F_{2\pi}(s, x) = \frac{G_{uz}(s, x + 2\pi)}{G_{uz}(s, x)} \quad (12)$$

It follows from the sensor configuration proposed in the previous section that we need to estimate the disturbance also at $x + \pi$. This is not possible with the same accuracy as in the previous case. It is due to the fact that the amplitude gain grows with x not linearly but with a (spatial) harmonic component with a period of about 2π . We fit a low-order rational function $\hat{F}_\pi(s)$ on $-\sqrt{F_{2\pi}(s, x)}$ to obtain at least a good estimate for the phase.

For a more efficient disturbance attenuation we shall put one additional sensor 4π upstream from the first sensor considered in the previous sub-section. It is far enough upstream from all panels so that the effect of wall transpiration on this sensor's measurements is negligible. It measures directly the oncoming wave-packet (assuming the measurement noise is negligible in the relevant frequency range). The model of $\hat{F}_{4\pi}(s)$ is computed the same way as that of $\hat{F}_{2\pi}(s)$. The overall disturbance transfer matrix from the shear measured far upstream to disturbance components at the other sensors is then given by

$$F(s) = \left(\hat{F}_{4\pi}(s) \begin{bmatrix} 1 & \hat{F}_\pi(s) & \hat{F}_{2\pi}(s) & \hat{F}_{2\pi}(s)\hat{F}_\pi(s) \end{bmatrix} \right)^T \quad (13)$$

The control configuration in the H_∞ control setting is in Fig 2. There are two sets of external inputs— w_1 disturbs the coprime-factor model, and w_2 which generates the flow disturbance measured at the far upstream sensor. It is filtered through $W_4(s)$ which passes only the frequencies in the growth region and enters the disturbance model $F(s)$ discussed in the previous section, and is fed to the controller as measurement y_1 . The measurements from the other sensors are in the other measurement y_2 . The penalized

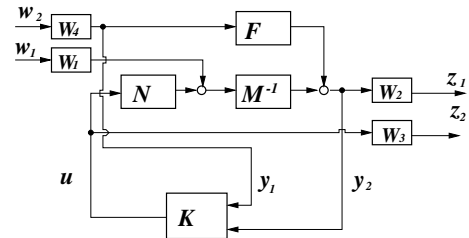


Fig. 2. Control configuration

outputs z_1, z_2 are filtered shear measurements and controls, respectively. Magnitudes plots of the frequency dependent weights are shown in Fig 3 (with all other details regarding the weight selection again given in [9]).

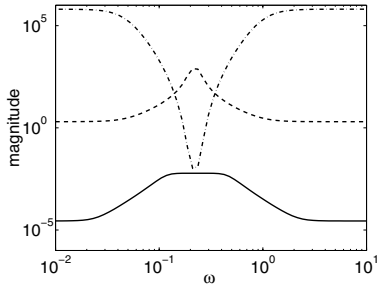


Fig. 3. Magnitudes of weights $w_2(s)$ (solid), $w_3(s)$ (dashed), $W_4(s)$ (dash-dotted)

For this weight combination, the model set is consistent with our extensive data set. To guarantee robust stability for this set of plants it is sufficient if the H_∞ performance index is less than 1. For the above problem formulation we found a controller which guarantees the H_∞ performance index $\gamma = 0.96$.

The plant order is 127; of those, 38 is the order of the model describing the relation between control and shear, order of the disturbance model is 13; the rest belongs to the weights. This will result in a controller of the same order, which is very high for implementation. However, it can be readily reduced by the standard Hankel-optimal reduction procedure to 30 which is practically feasible, without performance degradation. Reduction down to 20 results in a slight but acceptable performance degradation.

A. Initial Testing

In this section we shall consider the full-order controller. For the frequency-domain analysis, the disturbance has been simulated as an action of a blowing-suction panel (the same as those used for control) placed about 80π upstream from the panels. This shows that control action reduces shear magnitude significantly and slows its growth. Only the frequencies around the growth interval are shown—elsewhere, there is no significant difference between these two cases. Moreover, the design directly penalizes shear only at four points where the sensors are placed. These facts can be observed on the magnitude *versus* distance plot for fixed frequency ω in Fig 4. Notice, that here the magnitudes are scaled linearly. The positions of panels and sensors are shown in this figure.

III. 3D IMPLEMENTATION

A true test of ‘robust’ control in a fluid dynamics setting comes in the form of the control of three-dimensional disturbances. The control of coherent structures in the flow is of obvious benefit, particularly if the structures can clearly be identified as an active part of the transition process, see, for example, [10], [11]. Here we seek to apply the robust controller designed in the two-dimensional setting, to 3D disturbances in a three-dimensional flow. In particular a disturbance is initiated upstream in the flow by means of a blowing/suction panel of a short width in the spanwise

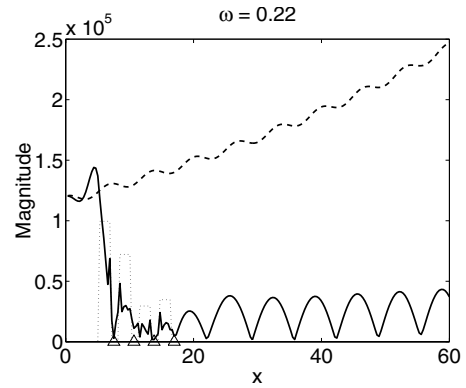


Fig. 4. Magnitude *versus* distance: controlled shear (solid), uncontrolled shear disturbance (dashed), control multiplied by 10^4 (dotted); triangles: positions of four sensors (the fifth-one is further upstream)

direction. This generates Tollmien-Schlichting type disturbances, which retain their two-dimensional characteristics downstream in the flow for values in the spanwise direction z , close to that of the initial disturbance. Indeed if the disturbance source was distributed completely across the span, then essentially only a two-dimensional disturbance would exist throughout the domain. However, as the disturbance propagates from the top edge of the disturbance source, three-dimensional characteristics of the disturbance arc outwards and propagate both in the z and x directions.

The streamwise-dimension of the 3D domain (see Figure 5) considered for the long channel lengths are 24π . The walls are located again at $y = -1$ and $y = +1$ and a spanwise (z) dimension of 20 non-dimensional units is considered. The boundary conditions for the spanwise limits consist of mirror symmetry conditions. This allows the placement of the generating panel pair at $z = 0$ to effectively double the domain considered in a spanwise sense to 40 non-dimensional units. Numerically the same resolutions in wall-normal and streamwise directions to that of the 2D case considered in the previous work are maintained. In the spanwise sense for the long-channel-length runs a relatively coarse resolution of 80 points across the span is used. This choice of resolution was based upon investigative simulations along a shorter channel length of 6π for finer and coarser resolutions.

For resolutions of 50% or lower than this, it was found that the 2D regions of the induced perturbation discussed below, no longer maintain their growth rates analogous to the purely two-dimensional cases of the previous section. In addition, two times and four times greater resolutions in the spanwise direction, were computed on still shorter channel lengths to observe inner three-dimensional perturbations, which are discussed elsewhere [12]. A non-dimensional time-step of 0.005 or smaller is used throughout, in keeping with the time step requirements found in the purely 2D setting of the previous work.

Mathematically the required time-varying boundary condition for the disturbance-generating panel pair can be given

by:

$$v(x, y = -1, z, t) = \begin{cases} f(t) & x \in [\frac{\pi}{2}, \pi] \text{ and } 0 \leq z < 2 \\ -f(t) & x \in [\frac{3\pi}{2}, 2\pi] \text{ and } 0 \leq z < 2 \\ 0 & \text{elsewhere} \end{cases} \quad (14)$$

where $f(t)$ is a prescribed time-varying amplitude. $f(t)$ is chosen so as to excite the 2D perturbation of $\omega = 0.2373$, that is $f(t) = \sin(t(0.2373))$.

An ad-hoc control scheme is devised based upon the previous MIMO scheme for the 2-dimensional channel. A series of rows of these 2-dimensional panel-pair-based controllers are spread spanwise across the channel as can be seen in Figure 6.

Each row is essentially an approximation of a two-dimensional problem, with the shear perturbation being measured in the center of each row. In an effort to maintain a practically realizable scheme, only a small number of rows are taken in the spanwise direction. There is no computational reason why each point in the spanwise direction couldn't be set up as an independent 2D controller however, this would be very far from being practicable. Although it is more practical to have fewer rows of greater width in the spanwise direction, the cost of this is that each row deviates further away from the 2-dimensional assumption. In the case that the flow differs abruptly in the spanwise direction, we may find that whilst a given row may be attenuating a disturbance on one side of the row, it may in fact be simultaneously amplifying disturbances on the other side.

Before the control was applied, the wall-shear-stress perturbation for this flow was taken across the entire bottom wall as can be seen again in Figure 7. Note that this figure makes use of the mirror symmetric boundary conditions, to double the effective span of the domain. It can be seen that the disturbance propagates in a similar fashion to a 2D disturbance for all points that share a spanwise coordinate with that of the disturbance-generating panel pair. As a result it makes obvious sense to place the first controller row of panels downstream of this generating panel pair of a panel width roughly the same width to that of the generating panel pair. The curvature of the wave then starts to increase slowly, and so a series of thinner rows are placed across the span.

The configuration used here consists of four independent rows (0–3) of the two-dimensional MIMO robust controller. The width of the first row is 4 in the spanwise direction. The widths of the remaining rows are all 2 respectively. The start of the first blowing/sucking panel pair for all rows is at 10π in the streamwise direction. Consequently the end of the last panel pair for each row is at 18π and sensor locations in the streamwise sense at 8.8π , 12.8π , 14.8π , 16.8π and 18.8π respectively. The sensor locations for each row in the spanwise sense are at the half width of each row, i.e. 2 for the row 0, 5 for row 1, 7 for row 2 and 9 for row 3. Figure 8 gives the result after control is applied.

Note that these rows of 2D controllers only measure the

shear stress perturbations at single points for each of the 5 sensor locations. As expected, each row acting on its sensor information attenuates its local approximation of a two-dimensional wave. Note that two adjacent rows may be blowing in opposite directions, e.g. rows 0 and 1 here. This will cause a sudden change in the shear-stress when the panels meet. Similar results to those given here have also been obtained for this case, and hence this simple extension of the controller designed for 2D disturbances can deal with at least this simple 3D perturbation.

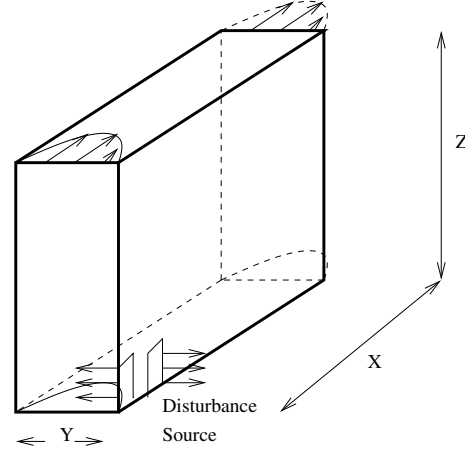


Fig. 5. Three-dimensional channel showing disturbance source on the lower wall.

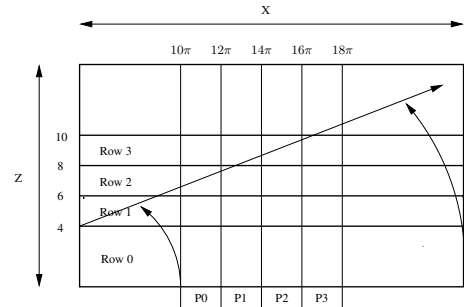


Fig. 6. Actuator configuration with four rows of the two-dimensional controller placed across the lower wall of the channel.

IV. CONCLUSIONS

This paper has considered the problem of robust control law design and evaluation for channel flow without the need to make a spatial periodicity assumption (as in previous work). A means of H_∞ based robust control law design has been given together with a sample result of this control law in action with a CFD simulator used as the real plant model.

The above results are for 2D flow and here the first results on the extension to the 3D case have been given. The complexity of the control law for the 2D case clearly suggests that this extension will be a non-trivial problem requiring

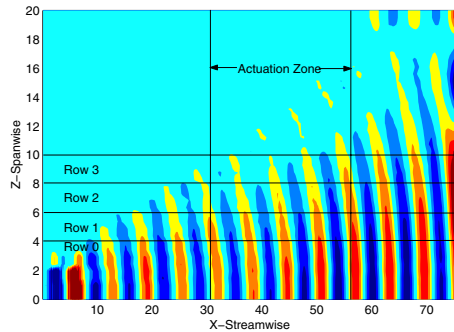


Fig. 7. Wall shear stress perturbation on the lower wall before the control is applied.

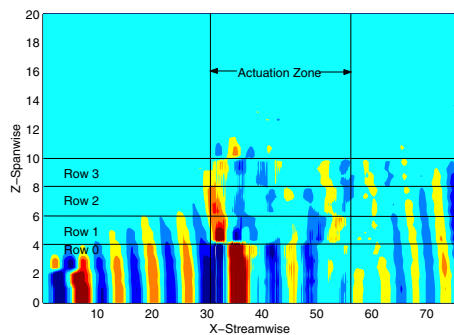


Fig. 8. Wall shear stress perturbation on the lower wall after the control is applied at a non-dimensional time of $t = 384$.

much further research. Here we have demonstrated that the control law designed for the 2D flow has some capability against 3D disturbances.

REFERENCES

- [1] S. S. Joshi, J. L. Speyer, and J. Kim, "A system theory approach to the feedback stabilization of infinitesimal and finite-amplitude disturbances in plane Poiseuille flow," *Journal of Fluid Mechanics*, vol. 332, pp. 157–184, 1997.
- [2] —, "Finite dimensional optimal control of Poiseuille flow," *AIAA Journal of Guidance, Control and Dynamics*, vol. 22, pp. 340–348, 1999.
- [3] T. R. Bewley and S. Liu, "Optimal and robust control and estimation of linear paths to transition," *Journal of Fluid Mechanics*, vol. 365, pp. 305–349, 1998.
- [4] L. Cortezzi, J. L. Speyer, K. H. Lee, and J. Kim, "Robust reduced-order control of turbulent channel flows via distributed sensors and actuators," in *Proc. of the 37th IEEE Conf. on Dec. and Contr.*, Tampa, 1998, pp. 1906–1911.
- [5] A. Balogh, W.-J. Liu, and M. Krstic, "Stability enhancement by boundary control in 2d channel flow—part i: Regularity of solutions," in *Proc. of the 37th IEEE Conf. on Dec. and Contr.*, Phoenix, 1999, pp. 2869–2874.
- [6] L. Baramov, O. R. Tutty, and E. Rogers, "Robust control of plane Poiseuille flow," pp. AIAA Paper 2000–2684, 2000.
- [7] J. Chen, "Frequency domain tests for validation of linear fractional uncertain models," *IEEE Transactions on Automatic Control*, vol. 42, pp. 748–760, 1997.
- [8] C. Canuto, M. Y. Hussaini, A. Quarteroni, and T. A. Zang, *Spectral Methods in Fluid Dynamics*. New York: Springer-Verlag, 1988.
- [9] L. Baramov, O. R. Tutty, and E. Rogers, " H_∞ control of non-periodic two-dimensional channel flow," *IEEE Transactions on Control Systems Technology*, vol. 12, no. 1, pp. 111–122, 2004.

- [10] N. Aubrey, P. Holmes, and J. L. Lumley, "The dynamics of coherent structures in the wall region of a turbulent boundary layer," *Journal of Fluid Mechanics*, vol. 192, pp. 115–173, 1986.
- [11] T. R. Bewley, P. Moin, and R. Teman, "DNS-based predictive control of turbulence: an optimal benchmark for feedback algorithms," *Journal of Fluid Mechanics*, vol. 477, pp. 179–225, 2001.
- [12] E. O'Dea, "Robust control of nonlinear 2D and linear 3D disturbances in channel flow by surface transpiration," Ph.D. dissertation, University of Southampton, England, 2004.